Supplementary Materials

Performance and mechanism of biobased-supported conjugated polymer donor with dual small-molecule acceptors

Houjin Luo[1,#], Linji Yang[1,#], Tingyong Yi[1,#], Misong Zhao[1,#], Guanqi Sun[1], Yuanyuan Kan[1], Guo Li[1], Ke Sun[1], Songlin Cai[1], Ke Xu[3], Junchao Jin[1,*], Xiaofei Wang[2,*], Tao Liu[1,*]

[1]School of Chemistry and Chemical Engineering, Guangxi Key Laboratory of Nonferrous Metals and Special Materials Processing, Key Laboratory of New Technologies for Nonferrous Metals and Materials Processing, Ministry of Education, State Key Laboratory of Featured Metal Materials and Life-cycle Safety for Composite Structures, School of Resources, Environment and Materials, Guangxi University, Nanning 530004, Guangxi, China.

[2]Institute of Eco-Environmental Research, Guangxi Academy of Sciences, Nanning 530007 China.

[3]Shenzhen Institute for Advanced Study, University of Electronic Science and Technology of China, Shenzhen 518110, China.

[#]Authors contributed equally.

Correspondence to: Dr. Tao Liu, Dr. Junchao Jin, School of Chemistry and Chemical Engineering, Guangxi Key Laboratory of Nonferrous Metals and Special Materials Processing, Key Laboratory of New Technologies for Nonferrous Metals and Materials Processing, Ministry of Education, State Key Laboratory of Featured Metal Materials and Life-cycle Safety for Composite Structures, School of Resources, Environment and Materials, Guangxi University, Nanning 530004, Guangxi, China. E-mail: p2025007@gxu.edu.cn; liutaozhx@gxu.edu.cn; Prof. Xiaofei Wang, Institute of Eco-Environmental Research, Guangxi Academy of Sciences, Nanning 530007, Guangxi, China. E-mail: wangxiaofei26@gxas.cn

Contents

1. Characterization Methods

Surface morphology of samples was investigated using scanning electron microscopy (SEM). Specific surface area was determined via nitrogen adsorption-desorption data and Brunauer - Emmett-Teller (BET) measurements. Absorption spectra of organic composite membranes and light absorption properties of pollutants were measured using a Shimadzu UV-3600 spectrophotometer. The separation efficiency of photogenerated carriers during photocatalysis in the composite material was determined via photoluminescence (PL) spectroscopy. The lifetime of excited electrons during photocatalysis in the composite material was measured using time-resolved photoluminescence (TRPL) spectroscopy. The photocurrent and electrochemical impedance of the material were recorded using an electrochemical workstation. In photoelectrochemical experiments, Ag/AgCl served as the reference electrode, a platinum electrode as the counter electrode, and Na_2SO_4 as the electrolyte. Intermediate products in the photocatalytic reaction system were identified using liquid chromatography-mass spectrometry (LC-MS). The work of key active species during photocatalytic reactions was conducted via electron spin resonance spectroscopy (ESR).

2. Adsorption properties of materials

Figure S5 illustrates the porous structure imaging of the catalyst observed under different resolutions through SEM, demonstrating its porous structure. This structure proves its high specific surface area and adsorption capacity, which contributes to its excellent physical adsorption performance.

3. Density functional theory (DFT) calculations and Fukui index

Density functional theory (DFT) calculations can accurately characterize the electrostatic potential distribution of PCP-Na and identify its reactive sites, providing theoretical basis for elucidating the degradation path of PCP-Na. As shown in Figure S6, PCP-Na molecular structure consists of benzene ring parent, hydroxyl substituent and five chlorine substituents.

Figure S8a shows the distribution characteristics of atomic-level electrostatic potential (ESP) of PCP-Na: red area corresponds to electron-deficient sites with low electron cloud density, blue area corresponds to electron-rich sites with high electron cloud density[1-3], among which the five chlorine substituents in electron-rich area are the main attack targets of H^+ and ·OH. Frontier orbital analysis shows that in Figure S8b, HOMO orbital electron cloud is mainly localized to the linking sites of benzene ring skeleton, hydroxyl functional group and chlorine substituent, suggesting that this region is vulnerable to electrophiles such as $\cdot O_2^-$ and ·OH. LUMO orbital electron cloud is concentrated in hydroxyl and benzene ring structural units, indicating that such sites tend to undergo nucleophilic reactions (such as ·OH attack).

Since HOMO/LUMO analysis is difficult to quantify the activity difference of each reaction site, this work further accurately locates the reaction active site of PCP-Na by Fukui function calculation. Figure S8d-f shows the Fukui index diagram of each atom in PCP-Na molecule: f^0 (free radical attack activity), f^+ (nucleophilic reaction activity) and f^- (electrophilic reaction activity). Fukui function analysis can directly reveal the interaction mechanism between reactive species and PCP-Na, and realize the accurate location of ROS attack sites. According to theoretical calculation results, atoms with higher f^0 values are easily attacked by ·OH atoms with higher f^+ values are easily targeted by $\cdot O_2^-$, and atoms with higher f^- values tend to react with H^+ .The data in Figure 6 show that O_{12}, Cl_7, Cl_8, Cl_9, Cl_{10} and Cl_{11} sites have high Fukui index[4], which confirms that hydroxyl functional groups and chlorine substituents of benzene ring in PCP-Na molecule are the main action sites of ROS, among which chlorine substituents can be attacked by $\cdot O_2^-$, h^+ and ·OH at the same time. This conclusion is in good agreement with the static potential distribution characteristics.

Table S1.*Langmuir kinetic model for pure CSC and three photocatalytic systems*

Catalyst type	Kinetic equation	lnQ_e	R^2
CSC	Q_t = 24.99617*(1 - exp(-0.09221*t))	3.3282	0.99965
PM6:IEICO-4F	Q_t = 26.51258*(1 - exp(-0.04787*t))	3.29722	0.99896
PM6:Y6	Q_t = 28.46115*(1 - exp(-0.03003*t))	3.66731	0.99737
PM6:IEICO-4F:Y6	Q_t = 32.02262*(1 - exp(-0.02548*t))	3.47948	0.99416

Table S2.*Quasi-second-order kinetic curve parameters for pure CSC and three photocatalytic systems*

Catalyst type	Kinetic equation	$1/Q_e$	R^2
CSC	t/Q_t=0.03378t+0.16315	0.03378	0.9974
PM6:IEICO-4F	t/Q_t=0.0297t+0.55432	0.0297	0.98627
PM6:Y6	t/Q_t=0.02226t+0.97056	0.02226	0.98708
PM6:Y6:IEICO-4F	t/Q_t=0.02062t+0.98308	0.02062	0.93445

Table S3.*Comparative Degradation Performance of PCP-Na on Different Photocatalysts*[5-9]

Types of photocatalysts	PCP-Na concentration	Catalyst concentration	Time of reaction	Remove rate
Bi_3O_4Br	40mg/L	1g/L	Light for 15 min and Dark for 60 min	92%
Graphene/TiO_2	50mg/L	0.2g/L	Light for 120 min and Dark for 30 min	97%
BWO-0.12	30mg/L	0.5g/L	Light for 60 min and Dark for 60 min	90%
OVs-b	10mg/L	1g/L	Light for 240 min and Dark for 60 min	80%
TiO_2/Sep	10mg/L	1g/L	Light for 140 min and Dark for 60 min	90%

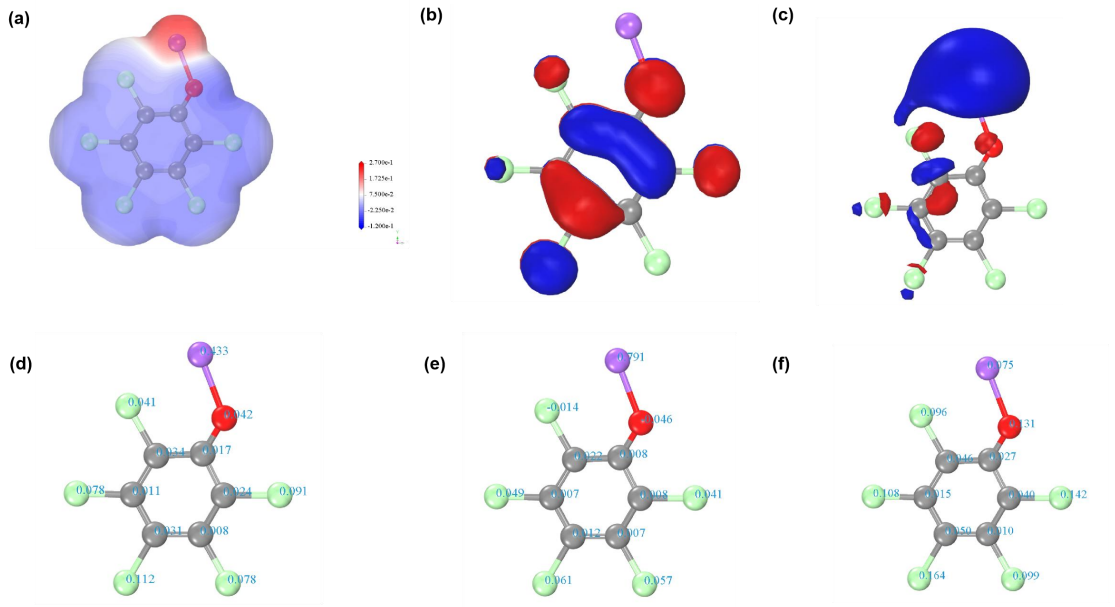

Figure S1. *(a) ESP diagram of PCP-Na, (b) HOMO distribution on PCP-Na, (c) LUMO distribution on PCP-Na, (d) f^0 of PCP-Na (e) f^+ of PCP-Na, (f) f^- of PCP-Na*

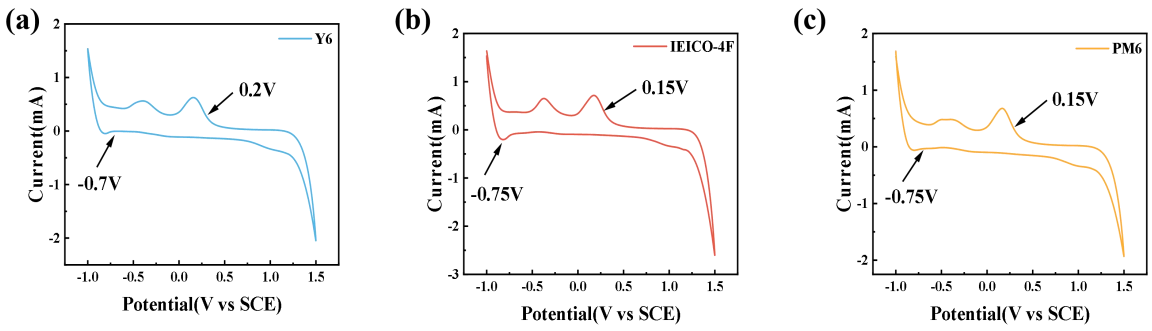

Figure S2. *Cyclic voltammetry (CV) curves of (a) Y6, (b) IEICO-4F, (c) PM6.*

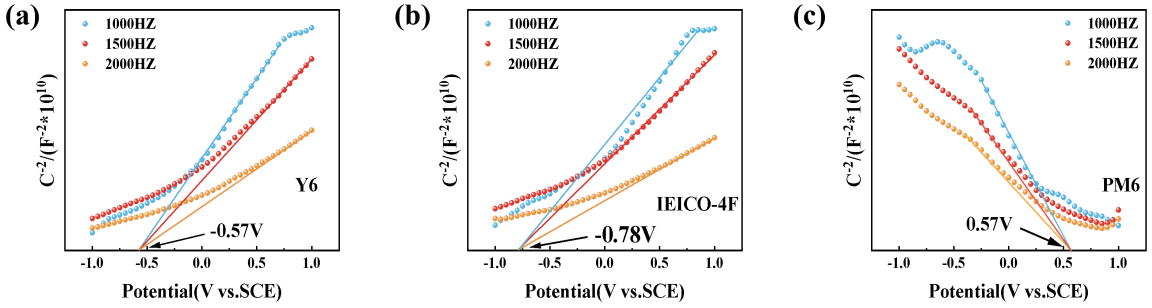

Figure S3. *Mott-Schottky characterization of (a) Y6, (b) IEICO-4F, (c) PM6.*

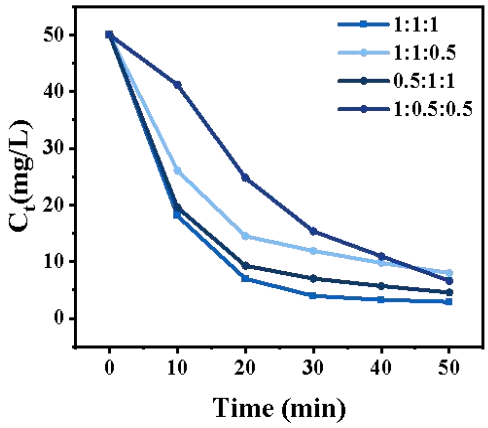

Figure S4.*Photocatalytic degradation curves of PCP-Na over composites with different donor–acceptor ratios.*

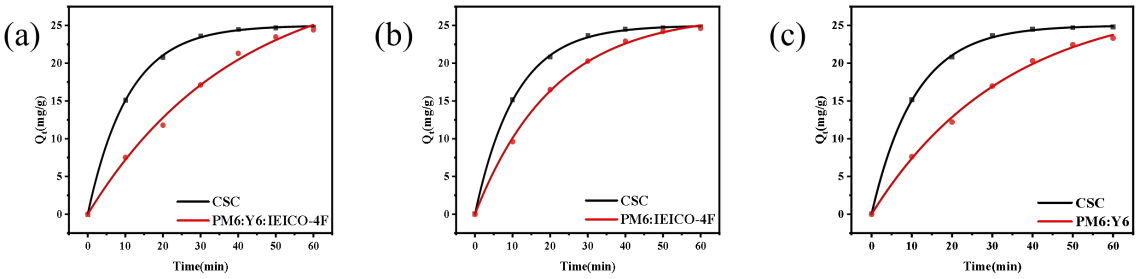

Figure S5. *(a) Langmuir kinetic model for pure CSC with PM6: Y6: IEICO-4F, (b) Langmuir kinetic model for pure CSC with PM6: IEICO-4F, (c) Langmuir kinetic model for pure CSC with PM6: Y6*

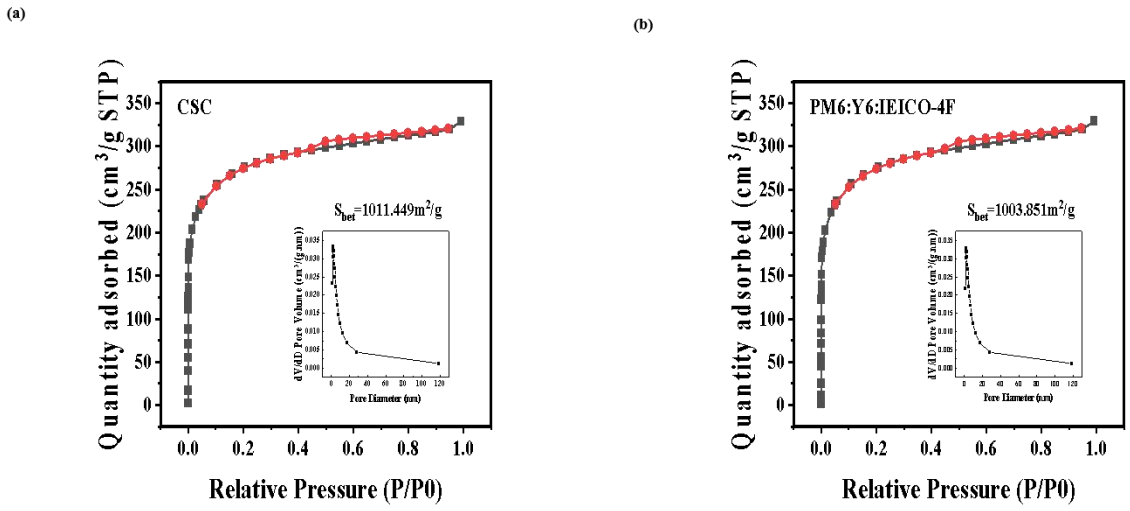

Figure S6. *(a) BET adsorption-desorption isotherm curve for pure CSC, (b) BET adsorption-desorption isotherm curve for PM6: Y6: IEICO-4F*

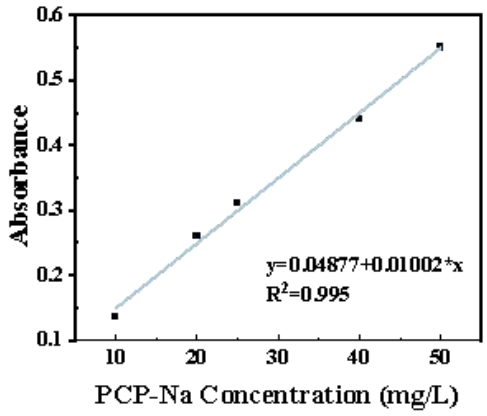

Figure S7. *Standard Calibration Curve of PCP-Na Solution Absorbance vs. Concentration*

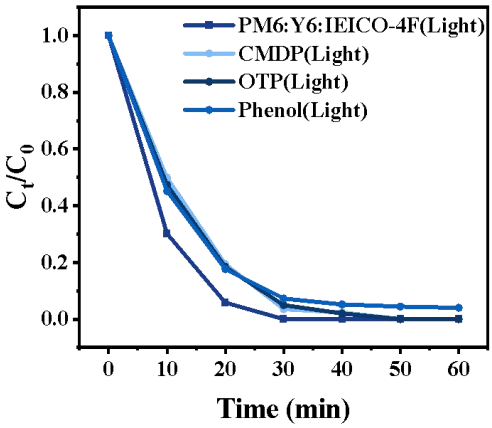

Figure S8.*Photocatalytic degradation profiles of different organic pollutants over the PM6:Y6:IEICO-4F composite under visible light irradiation.*

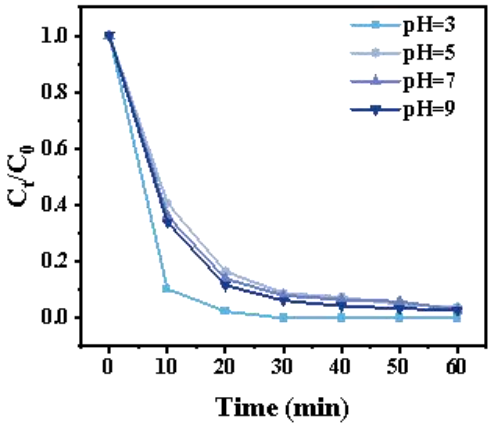

Figure S9. *Degradation performance of PCP-Na using PM6: Y6: IEICO-4F at different pH values*

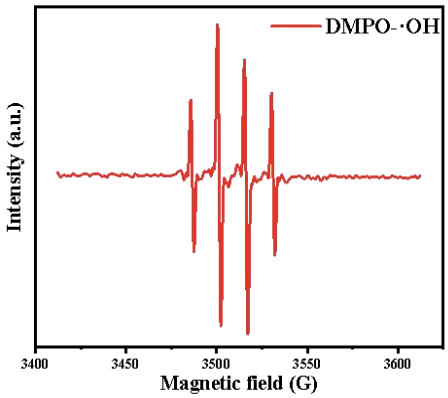

Figure S10.*EPR spectra of ·OH*

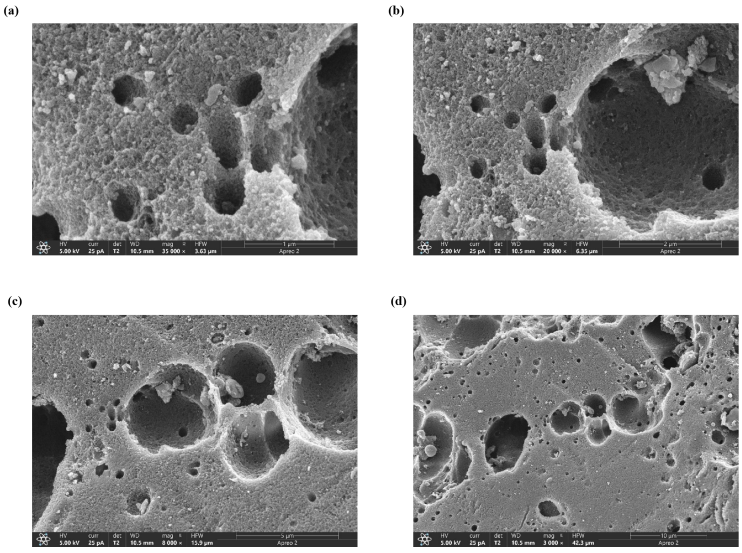

Figure S11. *Scanning electron microscope structural images of PM6:Y6:IEICO-4F at different magnifications: (a) 1 μm, (b) 2 μm, (c) 5 μm, (d) 10 μm*

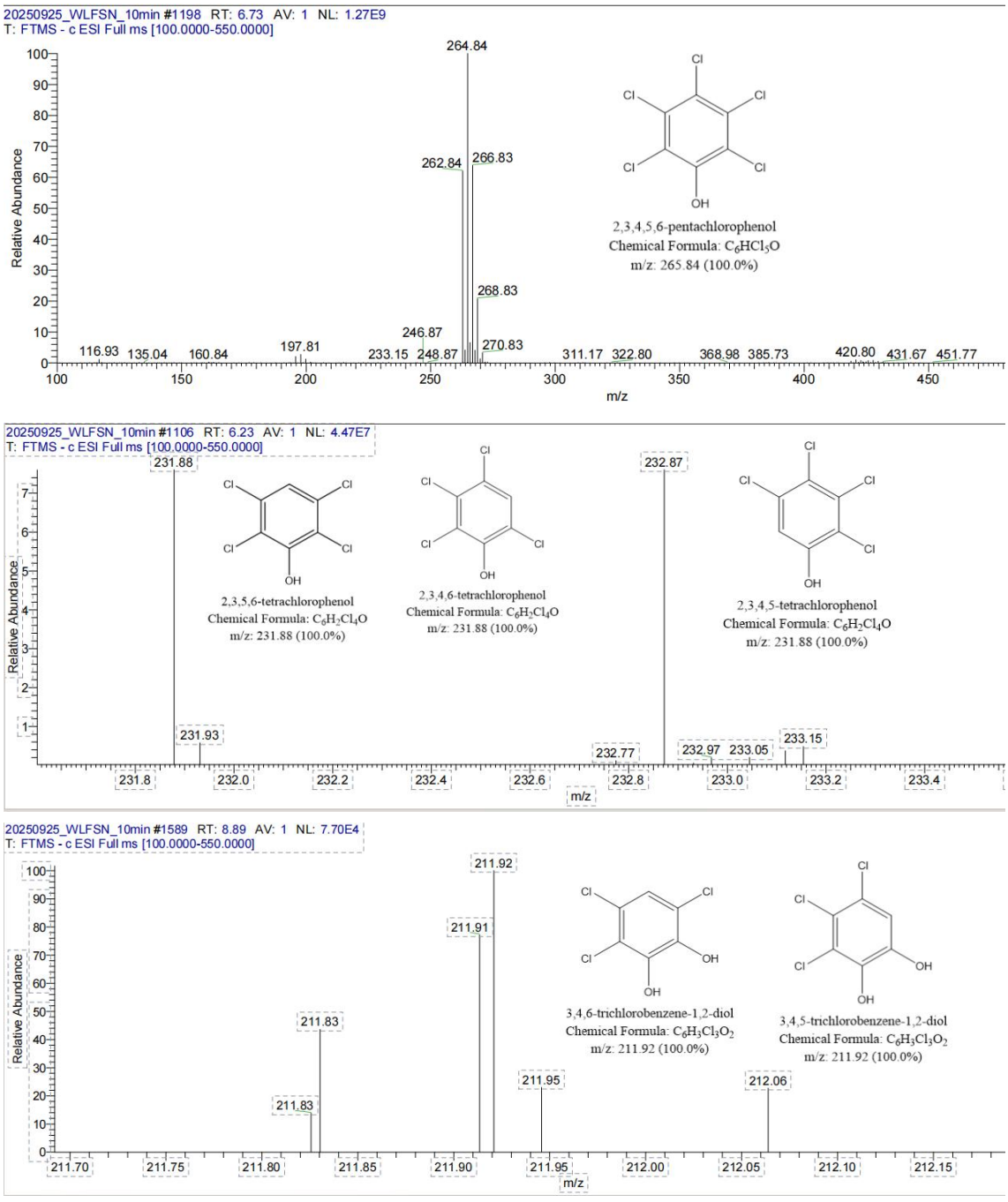

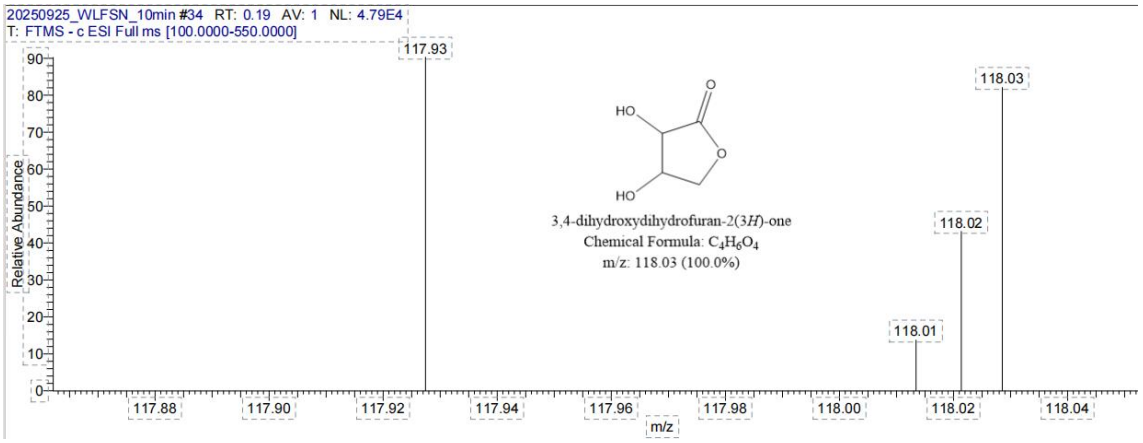
20250925_WLFSN_10min #34 RT: 0.19 AV: 1 NL: 4.79E4
T: FTMS - c ESI Full ms [100.0000-550.0000]
117.93
118.03
118.02
118.01
Relative Abundance
m/z
3,4-dihydroxydihydrofuran-2(3H)-one
Chemical Formula: C4H6O4
m/z: 118.03 (100.0%)

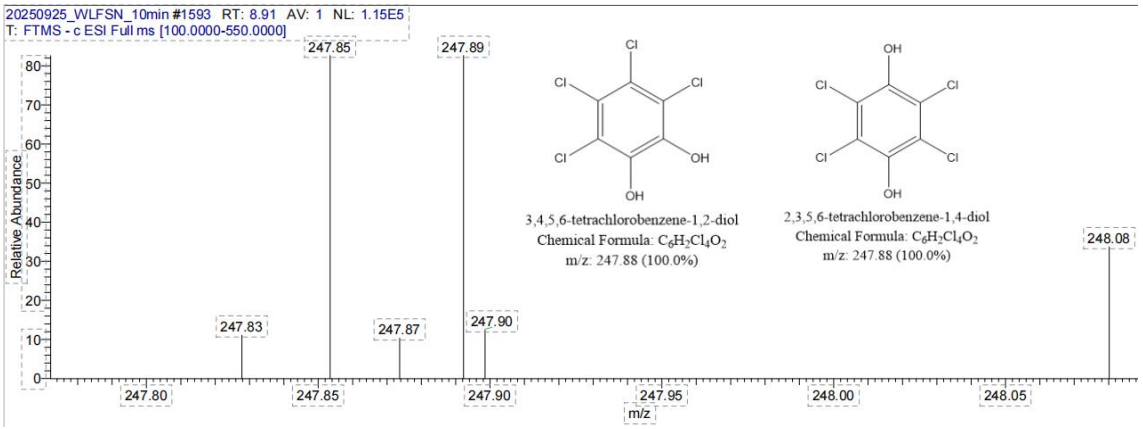
20250925_WLFSN_10min #1593 RT: 8.91 AV: 1 NL: 1.15E5
T: FTMS - c ESI Full ms [100.0000-550.0000]
247.85
247.89
247.83
247.87
247.90
248.08
Relative Abundance
m/z
3,4,5,6-tetrachlorobenzene-1,2-diol
Chemical Formula: C6H2Cl4O2
m/z: 247.88 (100.0%)
2,3,5,6-tetrachlorobenzene-1,4-diol
Chemical Formula: C6H2Cl4O2
m/z: 247.88 (100.0%)

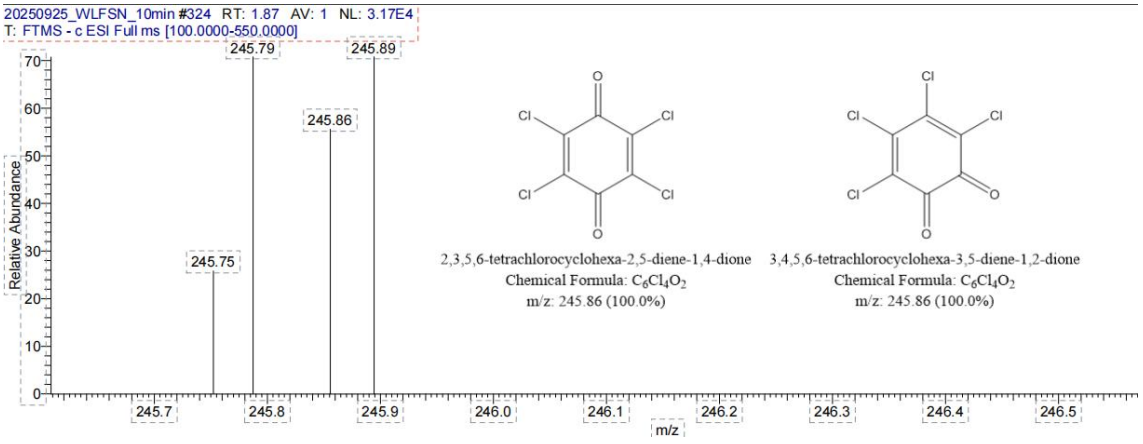
20250925_WLFSN_10min #324 RT: 1.87 AV: 1 NL: 3.17E4
T: FTMS - c ESI Full ms [100.0000-550.0000]
245.79
245.89
245.86
245.75
Relative Abundance
m/z
2,3,5,6-tetrachlorocyclohexa-2,5-diene-1,4-dione
Chemical Formula: C6Cl4O2
m/z: 245.86 (100.0%)
3,4,5,6-tetrachlorocyclohexa-3,5-diene-1,2-dione
Chemical Formula: C6Cl4O2
m/z: 245.86 (100.0%)

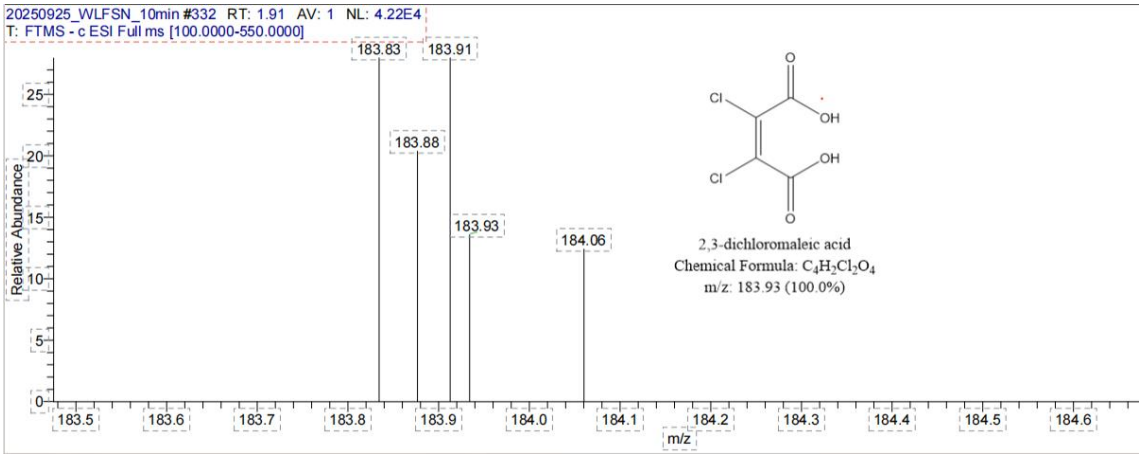
20250925_WLFSN_10min #332 RT: 1.91 AV: 1 NL: 4.22E4
T: FTMS - c ESI Full ms [100.0000-550.0000]
183.83
183.91
183.88
183.93
184.06
Relative Abundance
m/z
2,3-dichloromaleic acid
Chemical Formula: C4H2Cl2O4
m/z: 183.93 (100.0%)

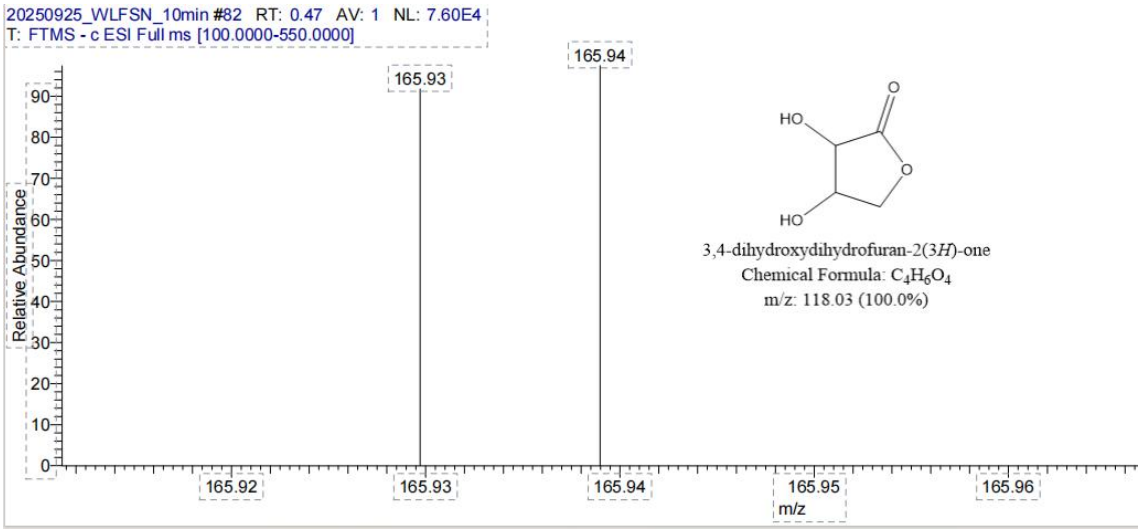
20250925_WLFSN_10min #82 RT: 0.47 AV: 1 NL: 7.60E4
T: FTMS - c ESI Full ms [100.0000-550.0000]
165.93
165.94
Relative Abundance
m/z
3,4-dihydroxydihydrofuran-2(3H)-one
Chemical Formula: C4H6O4
m/z: 118.03 (100.0%)

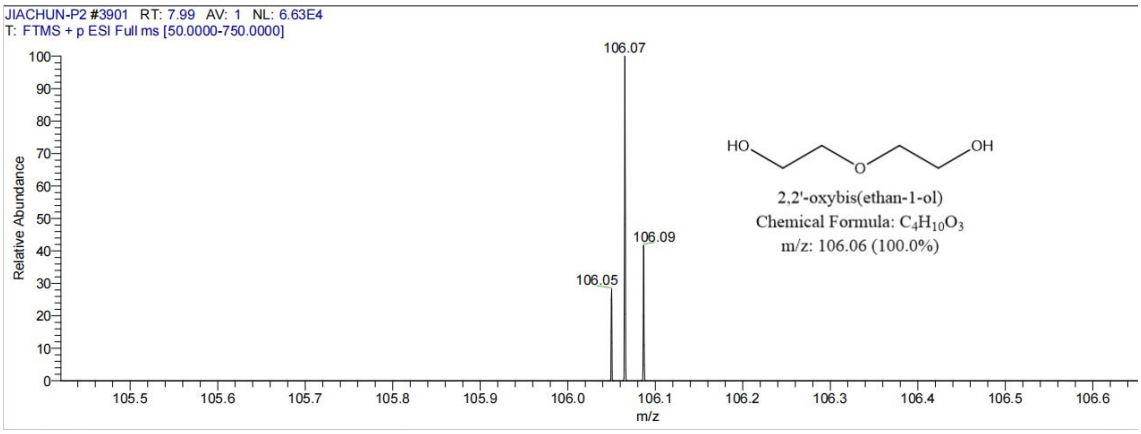
JIACHUN-P2 #3901 RT: 7.99 AV: 1 NL: 6.63E4
T: FTMS + p ESI Full ms [50.0000-750.0000]
106.07
106.09
106.05
Relative Abundance
m/z
2,2'-oxybis(ethan-1-ol)
Chemical Formula: C4H10O3
m/z: 106.06 (100.0%)

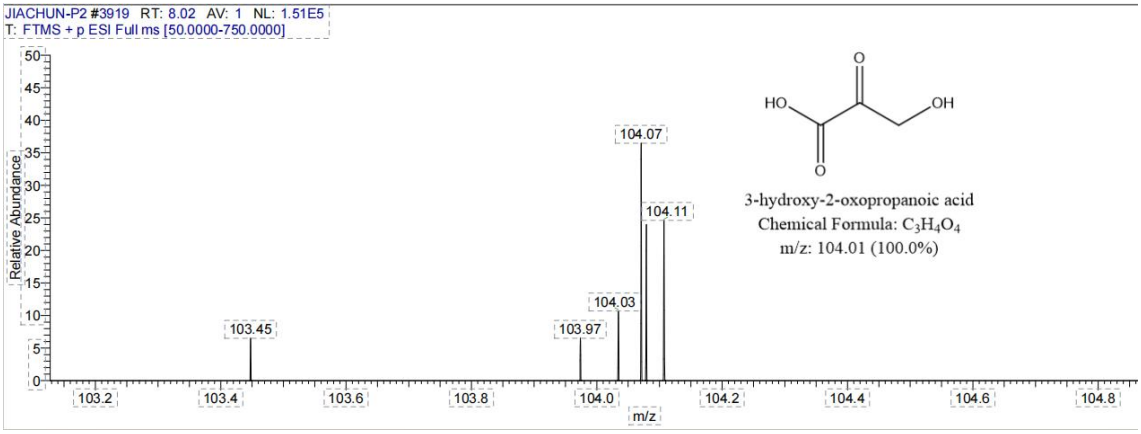
JIACHUN-P2 #3919 RT: 8.02 AV: 1 NL: 1.51E5
T: FTMS + p ESI Full ms [50.0000-750.0000]
104.07
104.11
104.03
103.45
103.97
Relative Abundance
m/z
3-hydroxy-2-oxopropanoic acid
Chemical Formula: C3H4O4
m/z: 104.01 (100.0%)

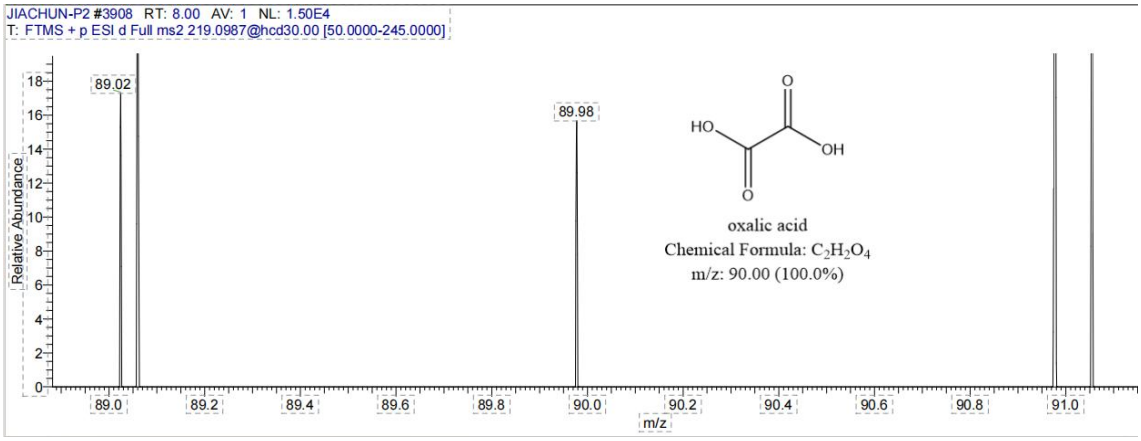
JIACHUN-P2 #3908 RT: 8.00 AV: 1 NL: 1.50E4
T: FTMS + p ESI d Full ms2 219.0987@hcd30.00 [50.0000-245.0000]
89.02
89.98
Relative Abundance
m/z
oxalic acid
Chemical Formula: C2H2O4
m/z: 90.00 (100.0%)

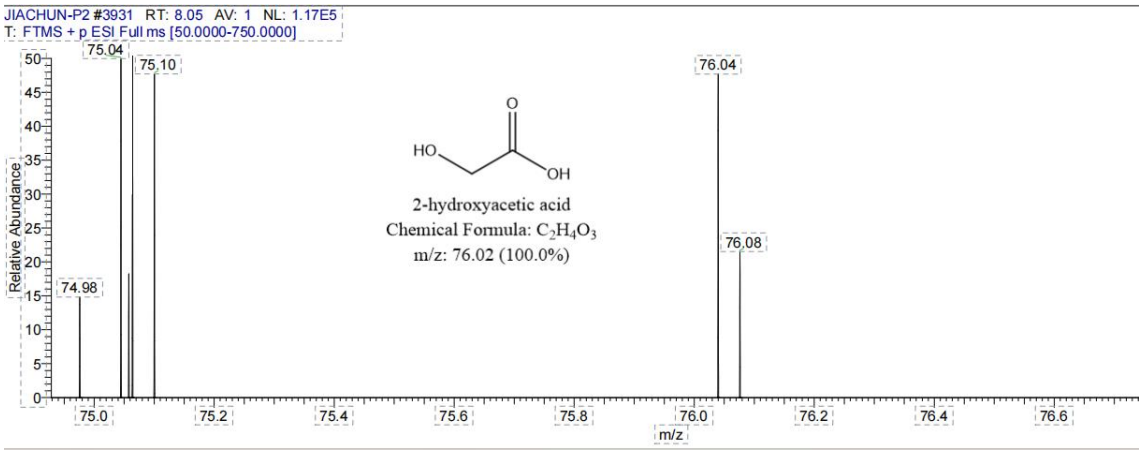

Figure S12. *Mass spectrometry of identified PCP-Na degradation intermediates*

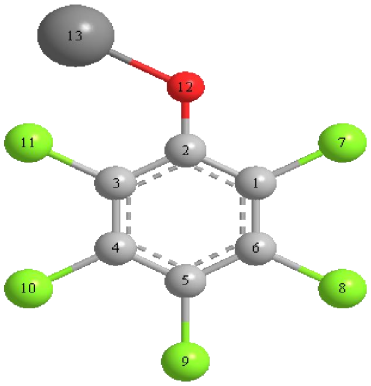

NO.	Atom	f^-	f^+	f^0
1	C	0.04	0.008	0.024
2	C	0.027	0.008	0.017
3	C	0.046	0.022	0.034
4	C	0.015	0.007	0.011
5	C	0.05	0.012	0.031
6	C	0.01	0.007	0.008
7	Cl	0.142	0.041	0.091
8	Cl	0.099	0.057	0.078
9	Cl	0.164	0.061	0.112
10	Cl	0.108	0.049	0.078
11	Cl	0.096	-0.014	0.041
12	O	0.131	-0.046	0.042
13	Na	0.075	0.791	0.433

Figure S13. *Fukui index of PCP-Na*

References

1. S. Cai, C. Huang, C. Wang, L. Zhang, K. Huang, H. Dong, H. Luo, K. Chen, S. Yao, H. Zhu, K. Sun, G. Li, T. Yang, B. Tang, B. Zou, and T. Liu: 'New breakthrough in dye removal: Ultrafast removal of high concentration MB with biochar-based organic photocatalysts under indoor light (30W/m2) drive', *Journal of Cleaner Production*, 2024.http://dx.doi.org/10.1016/j.jclepro.2024.141539

2. H. Yan, Y. Liang, T. Liu, C. Huang, S. Yao, H. Huang, Y. Peng, J. Xiong, K. Sun, H. Zhu, B. Zou, and S. Wang: 'Investigation of fullerene and non-fullerene materials in organic photocatalysts on the efficiency of photocatalytic degradation of polychlorinated biphenyls', *Journal of Colloid and Interface Science*, 2024.http://dx.doi.org/10.1016/j.jcis.2024.09.203

3. S. Cai, C. Huang, C. Wang, L. Zhang, K. Huang, H. Dong, H. Luo, K. Chen, S. Yao, H. Zhu, K. Sun, G. Li, T. Yang, B. Tang, B. Zou, and T. Liu: 'New breakthrough in dye removal: Ultrafast removal of high concentration MB with biochar-based organic photocatalysts under indoor light (30W/m2) drive', *Journal of Cleaner Production*, 2024, **449**.http://dx.doi.org/10.1016/j.jclepro.2024.141539
4. H. Yan, Y. Liang, T. Liu, C. Huang, S. Yao, H. Huang, Y. Peng, J. Xiong, K. Sun, H. Zhu, B. Zou, and S. Wang: 'Investigation of fullerene and non-fullerene materials in organic photocatalysts on the efficiency of photocatalytic degradation of polychlorinated biphenyls', *J Colloid Interface Sci*, 2025, **679**(Pt A), 10-20.http://dx.doi.org/10.1016/j.jcis.2024.09.203
5. J. Wang, Y. Yu, and L. Zhang: 'Highly efficient photocatalytic removal of sodium pentachlorophenate with Bi3O4Br under visible light', *Applied Catalysis B: Environment and Energy*, 2013.http://dx.doi.org/10.1016/j.apcatb.2013.02.009
6. Y. Zhang, Z. Zhou, T. Chen, H. Wang, and W. Lu: 'Graphene TiO2 nanocomposites with high photocatalytic activity for the degradation of sodium pentachlorophenol', *Journal of Environmental Sciences*, 2014.http://dx.doi.org/10.1016/j.jes.2014.08.011
7. S. Ge, D. Li, Z. Cui, Y. Zhang, S. Zhang, T. Zhang, G. Jia, W. He, and Z. Zheng: 'Regulating the relative content of O2− and OH for PCPNa degradation on BiOCl plates with controllable exposed crystal faces and surface oxygen vacancies', *Separation and Purification Technology*, 2019.http://dx.doi.org/10.1016/j.seppur.2019.115743
8. S. Wang, Z. Xiong, N. Yang, X. Ding, and H. Chen: 'Iodine-doping-assisted tunable introduction of oxygen vacancies on bismuth tungstate photocatalysts for highly efficient molecular oxygen activation and pentachlorophenol mineralization', *Chinese Journal of Catalysis*, 2020.http://dx.doi.org/10.1016/s1872-2067(19)63506-0
9. F. Zhou, M. Yang, R. Lu, and C. Yan: 'Simultaneous adsorption-photocatalytic treatment with TiO2-Sep nanocomposites for in situ remediation of sodium pentachlorophenol contaminated aqueous and soil', *Environmental Science and Pollution Research*, 2022.http://dx.doi.org/10.1007/s11356-022-18924-6